Article

Monitoring Forest Dynamics and Conducting Restoration Assessment Using Multi-Source Earth Observation Data in Northern Andes, Colombia

Carlos Pedraza [1,2]**, Nicola Clerici** [2,]*****, Marcelo Villa** [1]**, Milton Romero** [3]**, Adriana Sarmiento Dueñas** [3]**, Dallan Beltrán Rojas** [3]**, Paola Quintero** [4]**, Mauricio Martínez** [4] **and Josef Kellndorfer** [5]

[1] DreamGIS, Bogotá 110231, Colombia; carlos@dreamgis.com (C.P.); marcelo@dreamgis.com (M.V.)
[2] Department of Biology, Faculty of Natural Sciences, Universidad del Rosario, Bogotá 111221, Colombia
[3] 4D Elements Consultores, Bogotá 111321, Colombia; 4delements.consultores@gmail.com (M.R.); adrianasarmi@gmail.com (A.S.D.); sdallan.db@gmail.com (D.B.R.)
[4] Urra S.A E.S.P., Environmental Unit, Monteria 230002, Colombia; ambiental3@urra.com.co (P.Q.); mauriciojavier.ml@gmail.com (M.M.)
[5] Earth Big Data LLC, Woods Hole, MA 02543, USA; josef@earthbigdata.com
***** Correspondence: nicola.clerici@urosario.edu.co; Tel.: +57-313-348-57-26

Abstract: Examining the efficacy of current assessment methodologies for forest conservation and restoration initiatives to align with global and national agendas to combat deforestation and facilitate restoration efforts is necessary to identify efficient and robust approaches. The objective of this study is to understand forest dynamics (1996–2021) and assess restoration implementations at the Urra's supplying basin hydroelectric reservoir in Colombia. The processing approach integrates optical and radar Earth Observation (EO) data from Sentinel-2 and Landsat for forest mapping and multi-temporal forest change assessment (1996–2021), and a Sentinel-1 backscatter time-series analysis is conducted to assess the state of forest restoration implementations. The processing chain was scaled in a cloud-based environment using the Nebari and SEPPO software and the Python language. The results demonstrate an overall substantial decrease in forested areas in the 1996–2000 period (37,763 ha). An accuracy assessment of multi-temporal forest change maps showed a high precision in detecting deforestation events, while improvements are necessary for accurately representing non-forested areas. The forest restoration assessment suggests that the majority of the 270 evaluated plots are in the intermediate growth state (82.96%) compared to the reference data. This study underscores the need for robust and continuous monitoring systems that integrate ground truth data with EO techniques for enhanced accuracy and effectiveness in forest restoration and conservation endeavors.

Keywords: forest management; forest restoration; Sentinel-1; Sentinel-2; Landsat; time series; cloud computing

1. Introduction

In the context of the scientific and technical progresses in remote sensing, Colombia is taking advantage of the agreements made by the United Nations Framework Convention on Climate Change (UNFCCC) during the Conferences of the Parties in 2009 and 2010 (COP 15 and 16, respectively), and recently in Warsaw (COP 19), which require developing countries to establish national forest monitoring systems that allow for the quantification of greenhouse gas emissions and absorptions and changes in the extension of forests and forest carbon stocks. For this purpose, forest cover in Colombia was defined as "Land occupied mainly by trees that may contain shrubs, palms, *guaduas*, herbs and lianas, in which tree cover predominates with a minimum canopy density of 30%, a minimum canopy height (in situ) of 5 m at the time of identification, and a minimum area of 1.0 ha" [1]. The tree cover of commercial forest plantations, palm plantations, and trees planted for agricultural production are excluded. Deforestation is defined as "the direct and/or induced conversion

of forest cover to another type of land cover in a given period of time", and restoration is defined as "the recovery of forest cover in areas where it was not present in the past" [1]. These definitions are consistent with the criteria defined by the UNFCCC in its 11/COP 7 decision (FAO, Terms and definitions FRA 2020. 2020) and with the definition adopted by Colombia under the Kyoto Protocol.

Thus, in 2011, the governmental Colombian Forest and Carbon Monitoring System (SMByC) evaluated different remote sensing data processing techniques for the detection of forest cover and its respective changes over time, generating, as a result, the "Protocol for digital image processing for the quantification of deforestation in Colombia at the national level—coarse and fine scale" [1] which has been the methodological approach for the historical quantification of deforestation at the national level, e.g., for the 1990–2000, 2000–2005, and 2005–2010 periods and annually in the past decade from 2011 to 2022. These guidelines have become the Colombian standard for the evaluation of spatiotemporal forested and deforested dynamics, which is applied in the case of national regulations for companies that must report their effectiveness in protecting forests.

Since the first missions that integrated sensors on satellites to generate Earth Observation data, e.g., Landsat in 1972, a large number of orbiting missions have been launched for environmental applications with different characteristics, providing information that can be integrated into multiple applications to interpret land surface patterns and monitor changes in land use and land cover [2]. Satellite-based remote sensing has been proposed as an especially cost-effective way to provide reliable data on forest change dynamics [3–5]. Multiple methods have been developed based on satellite Earth Observation; nevertheless, there are limitations associated with each approach, including how to balance the integration of multiple sensors and the available resources for their implementation [6]. Some of these challenges are related to complex patterns and rapid changes associated with land cover trajectories [7–10], inconsistencies in Earth Observation data series among different missions [11], and, specifically in tropical areas, the continuous presence of clouds, which generate uncertainties in mapping tasks. The first launch of a global pathfinder optical mission with advanced observation strategies (i.e., Landsat) has been providing consistent EO data; however, it has the limitation of cloud interference. Recently, Synthetic Aperture Radar (SAR) sensors (e.g., ALOS-1 PALSAR-1 and Sentinel-1) have provided persistent data with the advantage of cloud-free EO data, which allow multiple challenges to be resolved in time series analyses to detect and quantify forest trajectories. In fact, the use of SAR sensors to generate EO imagery has increased in recent years in tropical regions, where radars provide day/night imagery without interference from atmospheric conditions [12–14]. This impulse has started in the past decade, mainly with the staging of ALOS-1 PALSAR-1, ALOS-2 PALSAR-2, and Sentinel-1 sensors, which can obtain EO data with a high acquisition frequency in the same area of interest when multiple missions are integrated in the analysis.

In Colombia, with respect to the increasing use of EO data from SAR sensors, most of the research has been focused on wetlands and flooding mapping [1,15–17], land use/land cover mapping (LULC) [18–20], and forest mapping and deforestation monitoring [21–24]. The growing application of EO data to monitor restoration has proven that this is a cost-effective means to select restoration sites and observe their progress over time [25], evaluate success and understand restoration recovery trajectories [26], generate specific restoration metrics [26] while monitoring vegetation structure trajectory to guide adaptive management [27], and determine specific spatial and temporal changes associated with degradation and recovery [28]. Nevertheless, with the increasing application of standardized protocols and methodologies based on remote EO data for restoration and forest monitoring, it is necessary to assess the level of uncertainty and their applicability in diverse regions facing multiple challenges, such as the Colombian Andes, which is characterized by almost permanent cloud cover and complex topographies, which may limit the application of EO data. The implementation of forest restoration initiatives is considered as one of the most promising climate actions to rapidly remove CO_2 from the atmosphere, especially in

tropical regions [29]; thus, analytical approaches based on remote sensing to monitor and assess forest restoration initiatives need to be improved.

The objectives of this work are as follows: (i) to detect forest change dynamics in a 25-year timeframe (the 1996–2000–2005–2010–2015–2021 period) based on optical sensors in area of influence of the hydroelectric dam (Colombia) based on national standards for forest and deforestation monitoring and (ii) to design a methodological approach to assess the status of forest restoration plots implemented as environmental offsets to compensate for impacts generated by the construction of the hydroelectric dam using a 5-year time series analysis of Sentinel-1 C-SAR imagery. Thus, this study proposes an operational monitoring and assessment approach for initiatives aimed to preserve forests, reduce deforestation, and restore forests by applying scalable and cost-effective technologies and methods.

2. Materials and Methods

2.1. Study Area

The study area, covering almost 89.000 ha, is located in the northwestern sector of Colombia, between 8°8′ N 7°47′ N and 76°27′ to 76°05′ W. It is characterized by an altitude ranging between 0 and 1250 m above sea level. Annual rainfall varies between 1.500 and 4.000 mm, with a dry season running from December to the end of March. The mean annual temperature fluctuates between 21.1 °C and 28 °C, with a warm semi-humid regime climate [30]. Within this region, three major biomes are identified: (i) The tropical wet zone biome covers 88% of the area and is the largest one, corresponding to areas where a humid rainforest predominates at elevations below 800 m above sea level (a.s.l.). (ii) The pedobiome of the tropical wet zone biome corresponds to areas where vegetation and flora types are determined by soil and humidity conditions [26]. This region is mainly represented by the Urra reservoir area, covering 9.3% of the region. (iii) The sub-Andean orobiome corresponds to an altitude range between 800 and 1800 m a.s.l., where a temperate climatic zone predominates along with the following humidity provinces: humid, semi-humid, and super humid [30].

The study area includes 90 villages within the municipalities of Tierralta and Valencia in the department of Córdoba and within Turbo, Apartadó, Carepa, and San Pedro de Urabá in the department of Antioquia. In 1996, the construction of the Urra hydropower facility, which collects the water of the Sinú river, began in the region, and the operations began in 2000 (Figure 1).
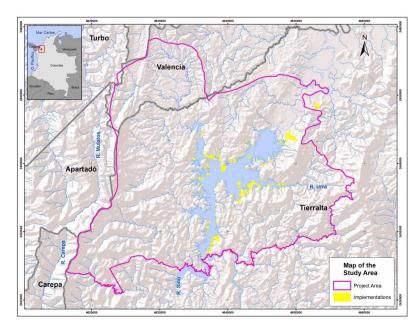

Figure 1. The study area around the influence region of the Urra hydropower project, located in Cordoba Department, Colombia.

2.2. EO from Passive (Landsat and Sentinel-2) and Active (Sentinel-1) Sensors

A 25-year (1996–2000–2005–2010–2015–2021) forest change analysis was performed based on the long-term availability of EO data from optical sensors (Landsat and Sentinel-2). The Landsat program has been providing continuous observations with 8- or 9-day repeat intervals for about 50 years [31], and it provides key advantages for long-term monitoring tasks, such as temporal and radiometric consistency throughout multiple Landsat programs [32]. To ensure a complete assessment from 1996 to 2021 could be conducted, multiple Landsat mission products were used, e.g., Landsat 5 TM, Landsat 7 ETM+, and Landsat 8 OLI, with a 30 m spatial resolution for visible and infrared bands. ESA Sentinel-2 MSI Level2A imagery was also included for the year 2021; imagery from this sensor was included to increase data availability by densifying the temporal coverage. Thus, revisit frequency can be improved from 8 or 9 days (based on Landsat) to 2.9 days (integrating Sentinel-2) [33], which contributes to this study by reducing spatial gaps caused by cloud cover, a major problem in Colombia. Also, Sentinel-2 imagery was integrated into the analysis to increase and improve the spatial resolution of thematic products through the generation of the 2021 forested/non-forested baseline, achieving a minimum mapping area between 0.25 and 0.5 ha, which was required to be decreased to a 1:50,000 scale for this study.

Landsat (Collection 2 Level-2) and Sentinel-2 (Level 2A) imagery was accessed through the Microsoft Planetary Computer platform (https://planetarycomputer.microsoft.com, accessed on 23 August 2023). All available imagery for each year with less than 50% cloud cover was transferred to the project's cloud-based storage infrastructure (AWS S3 bucket in the us-east-1 region). Based on all available imagery for each year, each band associated with a single acquisition was stacked to generate a multispectral multi-band image (Figure 2A). Cloud and shadow masking procedures were performed for each single acquisition scene from every dry season to generate a cloud-free mosaic for each year, avoiding atmospheric interference, especially during the rainy season [34]. Every pixel from the last acquisition of the corresponding year with the presence of clouds or mountain shadows was discarded and replaced by the closest cloud and shadow-free pixel to generate a yearly last pixel mosaic. The "last pixel" corresponds to the latest pixel acquired without cloud interference near the end of the year (31 December) for the corresponding year. Orthorectification and co-registration procedures were performed for the stacked images to obtain accurate georeferenced information (Figure 2A). To detect changes in the time series, it is key that the images are accurately co-registered and orthorectified so that the images acquired from different sensors and dates can be directly compared and processed; for the construction of the time series, it is essential to have an accurate pixel-level co-registration among all acquired images for each scene. This adjustment was performed by measuring the difference between pixels and re-projecting the coordinate of the displaced image ends in this same magnitude (considering that the downloaded images are in a projection system with metric units). The UTM projected reference system was maintained during the whole process until the final products to prevent the loss of co-registration between pixels when applying the geometric adjustments of the cartographic re-projection models.
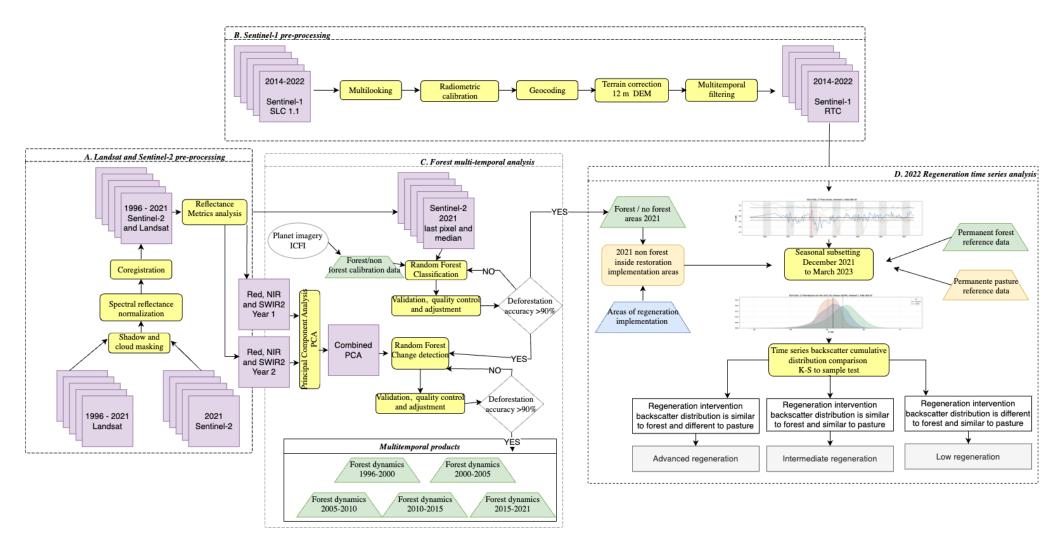
Figure 2. Processing workflow: (**A**) (optical pre-processing) and (**B**) (SAR pre-processing) describe all imagery pre-processing generated as inputs to be integrated in (**C**) to generate multitemporal analysis of forest dynamics, and (**D**) is used to assess restoration implementations around the Urra hydropower facility.

Precise reflectance and geometric image rectifications are necessary to generate quality data and to ensure the delivery of consistent products [35], and it is necessary to avoid measurement differences and false detections, i.e., due to geometric distortions or sensor calibrations. An adjustment to the radiometric signals of the images was thus performed to ensure consistency with each other (Figure 2A), i.e., through radiometric calibration, where digital numbers are transformed to surface reflectance, which, in the case of a tropical forest, is driven by species composition and vegetation structure characteristics [36]. Relative normalization was applied under the assumption that the relationship between the radiances recorded by the sensor on two different dates is spatially homogeneous (Figure 2A). In order to detect deforestation changes in multi-temporal forest dynamics analysis, a multivariate alteration detection algorithm, based on canonical correlation [37], was implemented, where the 2021 image was taken as baseline, and the rest of the images (1996, 2000, 2005, 2010, and 2015) were normalized with respect to this one. Quality control was carried out to ensure that the scenes were correctly co-registered and that they would allow effective multi-temporal analysis. This process guaranteed the use of different sensors and spatial resolutions so that they could be used in a homogeneous analysis.

Pan-sharpening techniques were employed on multi-year Landsat imagery (level 1) with spatial resolutions ranging from 15 to 30 m to facilitate fusion with Sentinel-2 data, which offer a higher spatial resolution at 10 m. Pan sharpening is a crucial preprocessing step aimed at enhancing the spatial details of lower-resolution multispectral imagery by integrating them with higher-resolution panchromatic imagery [38]. Through this process, we ensured compatibility and consistency between the Landsat and Sentinel-2 datasets, enabling seamless integration for subsequent analysis and interpretation. The application of pan-sharpening techniques not only preserves the spectral characteristics of Landsat imagery but also enhances its spatial resolution to match that of Sentinel-2 data, thereby facilitating comprehensive and accurate assessments of landscape dynamics over time. Pan sharpening was implemented with GDAL Pansharpen library (https://gdal.org/programs/gdal_pansharpen.html, accessed 20 August 2023) using the nearest neighbor resampling algorithm without weights. Procedures were applied to the Landsat-7 imagery due to the failure of the scan line corrector (SLC) [39], resulting in gap strips on the imagery and leading to 22% of the image being missing. A Phase II approach [39] was implemented, integrating multiple SLC-off scenes to fill the scan gaps by incorporating cloud-free pixels from the closest scenes.

The Copernicus Sentinel-1 mission launched by the European Space Agency (ESA) is based on a constellation of the two satellites, Sentinel-1A (launched in 2014) and Sentinel-1B (launched in 2016), with a revisit time of 12 days each, carrying a SAR C-band sensor on board. Sentinel-1 SAR imagery was available from the Alaska Satellite Facility (ASF) platform, a mirror of the ESA Scientific Sentinel-1 hub. All available data from May 2015 to June 2022 were accessed through the ASF-DACC data repository, which resides at an AWS S3 bucket in the us-west-2 region. Figure 2B summarizes the five methodological routines for preprocessing Sentinel-1 imagery, which allow the Single Look Complex (SLC) images to be converted into 12 m resolution multi-look geocoded images, radiometrically and terrain-corrected to generate gamma-naught backscatter intensity ($\gamma0$) images, obtained after pre-processing is performed with the Gamma® software V2.6 [40]. To reduce speckle effects associated with SAR imagery, an enhanced Lee multitemporal filter was applied to the VH polarization by means of least squares of the signal intensity in a kernel area of 3×3 pixels [41].

2.3. Forest Multi-Temporal Analysis

All surface reflectance imagery processed based on Sentinel-2 and Landsat data were used to generate annual median and last pixel metrics for the Red, NIR, and SWIR2 spectral bands, which are the most relevant in vegetation change analysis [42] (Figure 2C). A forested/non-forested map was generated for 2021 as baseline using a pixel-based supervised Random Forest machine learning algorithm (MLA) included on the sklearn.ensemble

Python module (V 1.4.1) [43] (Figure 2C). The Random Forest (RF) algorithm has been widely used in classifying remote sensing data [44–47], which generally handles noise and overfitting of the data well and has high data dimensionality [47]. The RF classifier was initially parameterized using training samples (250 forested and 275 non-forested point samples) generated based on the visual inspection of 2021 high-resolution Planet imagery of Red, NIR, and SWIR surface reflectance metrics (median and last pixel). Once the first version of the 2021 forested/non-forested map was generated by the RF classifiers, a visual assessment of the classified map was carried out using Planet imagery as quality control, validation, and adjustment procedure (Figure 2C). If deforestation accuracy of at least 90% was not obtained, new samples were generated in regions where misclassifications were observed. Then, the model was recalculated, and this process was iterated until a 90% accuracy was obtained (Figure 2C). Sample data and quality control procedures followed the forest definition from the Colombian Forest and Carbon Monitoring System (SMByC).

To derive multitemporal forest change products and estimate deforestation extent between for the 1996–2000, 2000–2005, 2005–2010, and 2015–2021 periods, a semi-automated RF approach was used (Figure 2C). For the change class, training points between 2015 and 2021 were generated based on a visual interpretation of deforested areas from Sentinel-2, Landsat, and Planet imagery. Red, NIR, and SWIR bands from 2021 and 2015 were combined into principal component bands within a single image (Figure 2C) and integrated as predictive variables in the RF model to identify highly and lowly correlated areas. Principal component analysis has been demonstrated to capture maximum variances in a finite number of orthogonal components based on eigenvector analysis from the correlation matrix, providing a robust and simple approach to generate input variables for change detection analysis [48]. The principal component bands generated based on two different years are highly correlated between unchanged areas (forested and non-forested stable areas), while a low correlation between significantly changed areas is expected (e.g., deforestation). The RF classifier was configured with the following parameters: n_estimators set to 100, representing the number of trees in the forest; criterion set to "gini" to measure the quality of a split based on Gini impurity; max_depth set to none to expand nodes until all leaves are pure or contain less than the specified minimum samples for splitting; and min_samples_split set to 2, indicating the minimum number of samples required for node splitting, with the option to set it as a fraction of the total number of samples. No weight was assigned to trees or predictable bands, and iterations continued until an output error of 5% was achieved. Once the first version of the 2015–2021 deforestation map was derived using the RF classifiers, a visual verification was performed by iterating validation, generating new training points and a new model until accuracies higher or equal than 90% for the deforestation class were obtained (Figure 2C). An accuracy threshold of 90% for the deforestation category was defined for the producer and user accuracy estimator to reduce the under and overestimation of deforested area. Once the expected accuracy was achieved, the forested/non-forested map of the following year (2015) and the change map (2015–2021) were updated. This process was repeated for each change period analyzed.

Sample-Based Estimation of Area and Accuracy

Due the importance of estimating forest, non-forest, and deforestation extent based on the thematic maps generated and the need for reproducible protocols for forest and deforestation mapping, an accuracy quantification is needed for reporting areas associated with each class of thematic maps [49]. A quantitative accuracy assessment for each class of thematic products was carried out to estimate and understand uncertainties on area estimation-based bias attributable to omission and commission classification errors. Olofsson et al.'s approach [50] was implemented for assessing and estimating land change product accuracy, since it is a well-accepted standard for land change accuracy assessment besides the national standard in Colombia implemented by the SMByC [42]. The initial validation sample size (n) was determined by setting the expected standard error

to Si = 0.01, the area proportions were mapped for each class, and theoretical validation user accuracy was defined by the SMByC standards for each class, i.e., 99 validation points were estimated for forested areas, 6 for deforested areas, and 129 for non-forested areas. Nevertheless, the final validation size per category was balanced to a total of 100 points for each class due to the low numbers obtained for deforestation class explained by the proportion area of this category. The spatial distribution of validation points was determined by an automated stratified random seed to ensure no bias due to the spatial distribution of validation points. Target user accuracy (U_i) was set to 0.9 for both stable forest and non-stable forest covers, since these classes are usually considered to have a high accuracy, while for the deforestation class, Ui = 0.8 was assigned.

2.4. Forest Restoration Status Assessment

Time series analysis using Sentinel-1 imagery was carried out to study vegetation seasonal variations and to assess the status of areas where restoration initiatives were implemented since 2014. The boundaries of the implementation areas of restoration by the Urra company were integrated (Figure 2D) and overlapped to the forested/non-forested areas of the thematic map for 2021 (Figure 2C). The masking process filters the non-forested areas within the intervention plots to perform a restoration status evaluation analysis (Figure 2D). For many biomes, seasonal stratification of the time series will improve the detection of change events, for example, when dry/wet season conditions introduce significant changes in backscatter due the presence of surface water or phenology variations [51]. In this sense, to minimize the influence of seasonal variation in the assessment of structural trajectories of restoration areas, a seasonal trend analysis was introduced in the assessment. Therefore, the first step was to subset the time series data by identifying the dry season to minimize the precipitation effects on backscatter levels. Dry season months were identified within the time series backscatter from Sentinel-1 from the years prior to 2021 (2017–2020); dry season (December to March) corresponds to yearly consistent low backscatter values that were validated with precipitation data [52]. Imagery from December to March was selected to be included in the analysis as the dry season period (Figure 3).
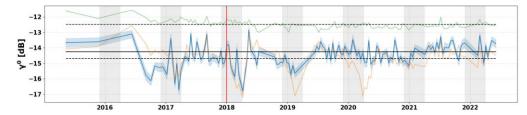

Figure 3. Sentinel-1 VH cross-polarization backscatter time series profile for assessed plot (blue line) with implementation year 2018 (vertical red line) contrasted with forest reference time series (green line) and pasture reference time series (yellow line). Dry season was defined as December to March (grey areas).

To assess the current state of the restoration process and determine if the current state of the vegetation structure is more similar to the reference coverages of well-preserved natural forests or, on the contrary, has a greater affinity with the backscatter response of the pastures, a comparative analysis of the dynamics of the vegetation structure from plots undergoing restoration was performed based on available Sentinel-1 time series data (Figure 2B). The assessment was based on a Kolmogorov–Smirnov test, which allows the distributions of the backscatter of the implementations to be compared with forest and pasture reference data, where the following hypotheses were proposed:

H0. *The sample of the radar signal backscatter of the regeneration plot and the sample from the reference data belong to the same distribution.*

H1. *The sample of the radar signal backscatter of the regeneration plot and the sample from the reference data DO NOT belong to the same distribution.*

A total of 270 polygons of intervened plots, which have different years of implementation of reforested and/or revegetated measures (2004–2010 and 2012–2018), were analyzed through a comparative analysis of the dynamics in the vegetation structure in plots undergoing restoration with respect to two types of reference areas: pasture and forest (Figure 4). Reference data were generated based on the visual inspection of multi-year optical imagery products from Landsat, Sentinel-2, and Planet (1996, 2000, 2005, 2010, 2015, and 2021). Forest reference data were defined as consistent forested areas identified in all years, and pasture reference data were defined as consistent pasture areas from 2005 to 2021.
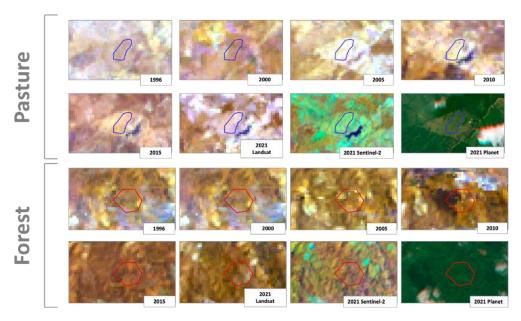

Figure 4. Optical imagery for multiple years was used to generate reference data for forest (red) and pasture (blue) polygons. Landsat and Sentinel-2 imagery correspond to the annual median values combined on NIR (red), SWIR (green), and Red (blue) bands. Planet Scope for December 2021 was obtained from the Visual Biannual Archive.

The cross-polarization VH backscatter values from the Sentinel -1 SAR sensor for the most recent dry period (2022) were used as proxies for the measurement of the structure of aboveground vegetation (i.e., tree height and canopy size). Multiple studies indicate that SAR cross-polarization (VH in the case of Sentinel-1 or HV in the case of ALOS-PALSAR) shows a higher correlation with biomass compared with co-polarization (VV in the case of Sentinel-1 or HH in the case of ALOS-PALSAR) to detect vegetation structure changes [53–57]. Backscatter from co-polarization is usually sensible to surface scattering components [57], and it is frequently applied to detect surface water [56].

A 95% confidence interval was chosen; therefore, if the *p*-value is less than 0.05 (or 5%), it provides sufficient evidence to reject the null hypothesis in favor of the alternative. This determines the status of the forest restoration implementation based on the following rules: (i) if it is in an incipient state, it has a greater similarity to pasture; (ii) if it is in an intermediate state, it has no similarity to pasture nor forest; and (iii) if it is in an advanced state, it has a greater similarity to forest (Figure 2D).

2.5. Computing Infrastructure

The Nebari open-source data science platform (https://www.nebari.dev/, v2023.5.1, accessed on 12 August 2023) was used to develop and implement Python routines for restoration assessment, integrating the Sentinel-1 time series backscatter generated us-

ing the proprietary software for Earth Big Data Processing, Prediction, Modeling, and Organization (SEPPO v5.0.0) to access the cloud Sentinel-1 imagery and perform all pre-processing procedures necessary to generate useful time series EO data for future analysis. The Nebari platform was configured by Earth Science Information Partners (ESIP; https://www.esipfed.org/ accessed on 12 August 2023), through the Earth Big Data LLC partnership, to run XLarge Instances (8CPU/32 GB), implementing a parallel computing auto-scaling approach with a maximum of 20 workers (CPU).

3. Results

3.1. Optical and Radar Imagery Processing

The images correspond to those available in the second half of the year corresponding to the analysis date. For example, for the analysis of the year 2010, imagery from 1 July to 31 December 2010 was selected to obtain a composite for this year from the historical series of images, metrics, and statistics. A total of 63 images were obtained for the 1996–2021 period to generate the yearly median and last pixel partially cloud-free mosaics for the Red, NIR, and SWIR bands (Figure 5); some pixels for specific years consistently presented the presence of clouds.
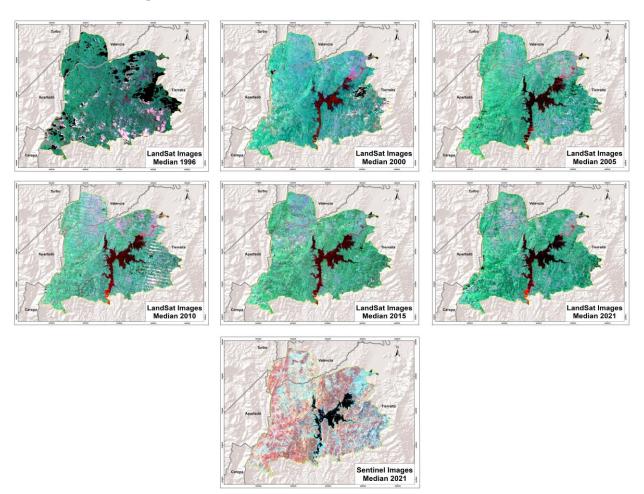

Figure 5. Optical pre-processing results for Sentinel-2 (2021) and Landsat (1996, 2000, 2005, 2010, 2015, and 2021) imagery. The mosaics generated correspond to annual median values combined on NIR (red), SWIR (green), and Red (blue) bands.

A total of 285 Sentinel-1 radiometric and terrain-corrected images were used for the 2014–2022 period, of which 136 correspond to Sentinel-1A and 149 correspond Sentinel-1B, providing Earth's surface observations every six days (Figure 6). All images, with a final spatial resolution of 12 m, were stacked in Zarr files, a Python library for chunked,

compressed, and parallelized N-dimensional arrays (Figure 6), providing a flexible and scalable approach to store large datasets in a compressed format, allowing for the efficient storage and retrieval of data in a cloud-based computing environment.
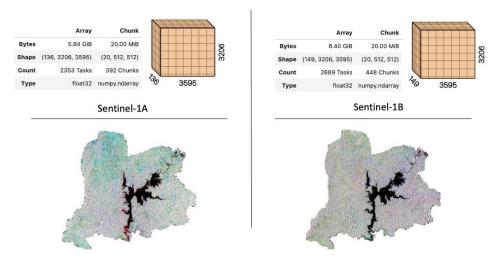

Figure 6. Sentinel-1 radiometric and terrain products obtained from pre-processed imagery from both satellites (S-1A and S-1B). Single images were stacked in multidimensional time series array of earth observations.

3.2. Forested and Deforested Spatiotemporal Dynamics Using Optical Sensors

Based on the analysis of the forested/non-forested maps for the year of 1996, it was found that the initial baseline for forested areas covered a significant portion of the study area, corresponding to 45,186.9 hectares, which represents 50.7% of the total area. The remaining 49.3% of the area is represented by non-forested areas. However, when examining the dynamics of forest coverage change from 1996 to 2021 (Figure 7), a noticeable decreasing trend in forested areas was found.
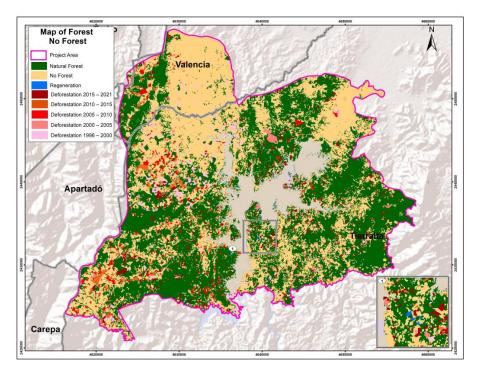

Figure 7. Map of forested, non-forested, deforested, and restored forest areas between 1996 and 2021 in the study area. Different red areas represent deforestation events during different periods.

Through the analyzed period, the reported forested area experienced a decline, decreasing from 43,350 ha in the 1996–2000 period to 37,763 ha in the 2015–2021 period. Concurrently, the extent of deforestation increased from 1837 ha in the 1996–2000 period to 2178 ha in the 2015–2021 period. In contrast, non-forested areas expanded, growing from 44,004 ha in the 1996–2000 period to 49,223 ha in the 2015–2021 period (Figure 8).
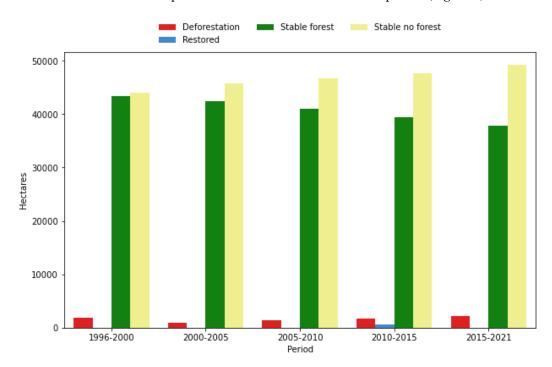

Figure 8. Estimated extent of forest change dynamics (hectares) for each of the periods analyzed (1996–2021).

Notably, the analysis also identified reforested and/or revegetated areas, which were first reported in the last two analysis periods. A total of 583 hectares were recorded by the year 2015, and an additional 27 hectares were identified by the year 2021, representing restored forested areas. By the year 2021, forests constituted 42.4% of the study area, covering a total of 37,789 hectares. The remaining 57.63% of the area consisted of non-forest coverages, accounting for 51,401 hectares (Figure 8).

Validation of Forest Change Dynamics for 1991–2021 Products

Table 1 shows the locations of the 300 points that served as samples for the validation of the forest surface change maps for the analyzed study periods. These points were spatially randomly generated for each of the classes: forest, non-forest, and forest loss. No validation points were integrated in the accuracy assessment approach for the reforestation category, as these areas represented a minimal percentage of the study area, and the areas were concentrated in specific sites that were completely visually inspected.

The classification accuracy assessment revealed variations in the performance of the maps across different time periods (Table 1). Table 1 shows that during the 1996–2000 period, the overall accuracy of the forest change map was 89%, the user's accuracy for the forest class was 78%, and the producer's accuracy for the forest class was 96%. Conversely, the non-forest class achieved a user's accuracy of 100% and a producer's accuracy of 80%. The deforestation class exhibited a user's accuracy of 90% and a producer's accuracy of 95%. In the subsequent period, spanning 2000–2005, the overall accuracy of the map improved to 96% compared with the change map for the 1996–2000 period. The user's accuracy for the forest class was 93%, indicating a high percentage of correctly classified forest pixels. Additionally, the producer's accuracy for the forest class was 98%, suggesting that the map accurately represented the distribution of forested areas. The deforestation class

presented a user's accuracy of 95% and a producer's accuracy of 99%, indicating the map's effectiveness in detecting and representing deforestation events. The non-forest class user's accuracy was 98%, and the producer's accuracy was 90%, indicating a slight overestimation of non-forested areas in the map. These results demonstrate the improved accuracy and reliability of the map in capturing land cover changes during this specific period compared to the 1996–2000 period.

Table 1. An accuracy assessment sample for the 1996–2000, 2005–2010, 2010–2015, and 2015–2021 periods' forested/deforested/non-forested maps for the area of influence of Urra's hydropower facility. The map categories are rows, while the reference categories are columns. The accuracy measures are presented with a 95% confidence interval.

Class	Forested	Deforested	Non-Forested	Total	Wi (%)	User's	Producer's	Overall
1996–2000								
Forested	78	4	18	100	0.38	0.78 ± 0.4	0.96 ± 0.3	0.89
Deforested	3	90	7	100	0.2	0.90 ± 0.02	0.95 ± 0.04	
Non-Forested	0	0	100	100	0.42	1 ± 0.4	0.8 ± 0.5	
Total	81	94	125	300	1			
2000–2005								
Forested	93	1	6	100	0.48	0.93 ± 0.4	0.98 ± 0.4	0.96
Deforested	0	95	5	100	0.01	0.95 ± 0.01	0.99 ± 0.01	
Non-Forested	2	0	98	100	0.51	0.98 ± 0.5	0.9 ± 0.5	
Total	95	96	109	300	1			
2005–2010								
Forested	92	0	8	100	0.46	0.92 ± 0.4	0.99 ± 0.4	0.95
Deforested	0	99	1	100	0.02	0.99 ± 0.01	0.98 ± 0.02	
Non-Forested	1	0	97	100	0.52	0.97 ±0.5	0.92 ± 0.5	
Total	93	101	106	300				
2010–2015								
Forested	92	1	7	100	0.45	0.92 ± 0.4	0.97 ± 0.4	0.95
Deforested	0	95	5	100	0.2	0.95 ± 0.1	0.99 ± 0.02	
Non-Forested	3	0	97	100	0.53	0.97 ± 0.5	0.89 ± 0.5	
Total	95	96	109	300				
2015–2021								
Forested	92	1	7	100	0.43	0.94 ± 0.4	0.97 ± 0.4	0.96
Deforested	0	95	5	100	0.2	0.94 ± 0.02	1 ± 0.02	
Non-Forested	3	0	97	100	0.55	0.97 ± 0.5	0.89 ± 0.5	
Total	95	96	109	300				

For the 2005–2010 period, the overall accuracy of the map remained consistently high at 95%. The user's accuracy for the forest class was 92%, indicating a high level of agreement between the map classification and the actual forested areas. The producer's accuracy for the forest class was 99%, suggesting that the map accurately represented the distribution of forest pixels. The deforestation class's user's accuracy was 99% with a producer's accuracy of 98%, indicating the map's effectiveness in detecting and representing deforestation events with a high level of precision. The non-forest class showed a user's accuracy of 97% and a producer's accuracy of 92%, suggesting a slight overestimation of non-forested areas in the map. These results highlight the accuracy and reliability of the map in capturing land cover changes during this specific time period.

From 2010 to 2015, the overall accuracy of the map remained consistently high at 95%. The user's accuracy for the forest class was 92%, indicating a high percentage of correctly classified forested pixels. The producer's accuracy for the forest class was 97%, indicating that the map accurately represented the distribution of forested areas. The deforestation class achieved a user's accuracy of 95% and a producer's accuracy of 99%, demonstrating

the map's effectiveness in identifying and representing deforestation events. The non-forest class demonstrated a user's accuracy of 97% and a producer's accuracy of 89%, suggesting a slight underestimation of non-forested areas in the map.

In the most recent time period analyzed, spanning 2015–2021, the overall accuracy of the map remained consistently high at 94.7%. The user's accuracy for the forest class was 92%, indicating a high percentage of correctly classified forested pixels. The producer's accuracy for the forest class was 97%, suggesting that the map accurately represented the distribution of forested areas. The deforestation class achieved a user's accuracy of 95% and a producer's accuracy of 100%, demonstrating the map's effectiveness in detecting and representing deforestation events. The non-forest class showed a user's accuracy of 97% and a producer's accuracy of 89%, indicating a slight underestimation of non-forested areas in the map.

3.3. Restoration Implementation Assessment Using Sentinel-1

The previous analysis of the forested/non-forested dynamics showed that three of the implementation plots were found to reach a completed forest succession state, indicating that, as of the analysis cutoff date in March 2022, these specific plots exhibited forest coverage in accordance with the definition provided by the SMByC.

Based on the time series analysis performed using VH polarization from Sentinel-1, cumulative distributions derived for each of the 270 implementation areas were contrasted to forest and pasture reference data (Figure 9). The two-sample Kolgomorov–Smirnov test revealed that 16 plots (5.93%) demonstrated an incipient restoration state, as evidenced by the vegetation structure estimates that displayed a greater resemblance to grassland areas compared to forests (Figure 10 provides an incipient example). Among the intervened plots subjected to evaluation (totaling 224), a significant majority of 82.96% (Table 2) was found to be in an intermediate state of the restoration process. These plots did not exhibit significant differences when compared to the two reference coverages: grasslands and forests (Figure 10 exemplifies the intermediate state). Furthermore, 27 of the evaluated plots, accounting for 10% of the total (as outlined in Table 2), displayed significant differences compared to the grassland reference data, but they did not exhibit significant differences in comparison to forests. Consequently, these plots were classified as being in an advanced state of reforestation (Figure 10).

Table 2. Results of restoration state assessment for 2022 dry season for 270 implementation plots evaluated based on Sentinel-1 VH backscatter.

Regeneration State	Number of Implementations
Incipient	16
Intermediate	224
Advanced	27
Completed	3

When the number and state of restoration were inspected in relation to the implementation years, some years showed a higher number of implementation plots in an advanced state of restoration. The years 2018, 2016, 2013, and 2014 demonstrated a substantial presence of seven, five, five, and four plots in the advanced state, respectively. Additionally, the year 2008 showed two plots in the advanced implementation state, while for the years 2009, 2012, 2015, and 2017, each one had a single plot in this state (Supplementary Figure S1 and Table S1).

No implementation plots from the years 2004, 2005, 2006, 2007, and 2010 were observed to achieve an advanced state in the restoration process. Instead, most plots from these years exhibited intermediate states within the reforestation process, indicating ongoing progress towards full restoration. To explore the relationship between the restoration state and the implementation year, a Chi-squared test was performed. The results of the test indicated that there is no statistically significant association between the restoration state

and the implementation year (Chi-squared statistic: 44.2823; degrees of freedom: 39; and *p*-value: 0.2586), suggesting that the restoration state is independent of the specific year of implementation.
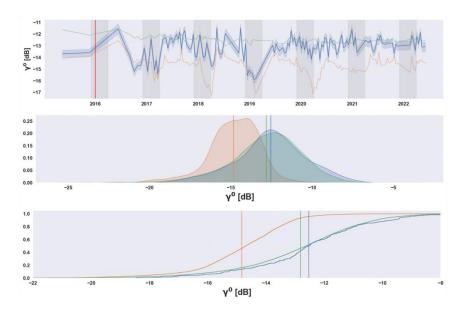

Figure 9. **The** Synthetic Aperture Radar (SAR) time series mean cross-polarized (VH) backscatter values (**top**) and cumulative distributions (**middle** and **bottom**) associated with reference areas, forest (green) and pasture (orange) areas, and assessed implementation plots (blue). This implementation was classified as being in an advanced state of restoration where the cumulative distribution is closer to the forest distribution. The implementation of the restoration date (red) and dry season period (December, January, February, and March) (grey) are included.
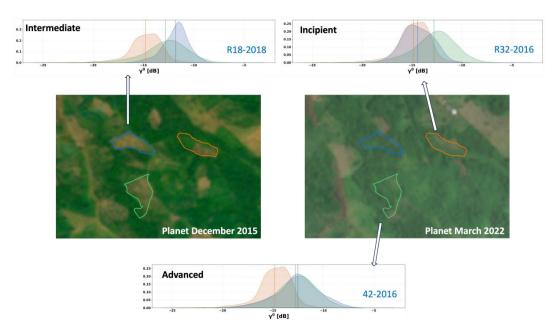

Figure 10. An assessment of three implementation plots based on the backscatter cumulative distributions and reference data for the 2022 dry season. The 42-2016 plot (green polygon) exhibited similarity to the forest reference (green backscatter distribution). The R18-2018 plot (blue polygon) indicated an intermediate restoration state due to differences in the backscatter distribution (blue) compared to forest (green backscatter distribution) and pasture (orange backscatter distribution). The R32-2016 plot (orange polygon) exhibited similarity to the pasture reference (orange backscatter distribution).

4. Discussion

4.1. Forested and Deforested Spatiotemporal Dynamics Using Optical Sensors

The results demonstrate that the proposed method allows for an efficient identification of forest loss within the study area. The developed method enables the detection of changes occurring within forest coverage, providing a quantitative measure and the spatial locations of the observed change events. This is achieved through the creation of composite images that reduce areas without information and extract pixels to generate information-rich images, removing the gaps generated by clouds and sensor malfunctions [30,49]. In accordance with a national [1] deforestation spatiotemporal trend analysis, this research reveals the highest deforestation trend during the period from 1996 to 2000. The initial baseline in 1996 showed that forests covered a significant portion of the study area, accounting for 50.7% of the total area. However, over the analyzed period, there was a noticeable decrease in forested areas, with a corresponding increase in non-forested areas. Deforestation played a significant role in this trend, as forested areas declined from 43,350 hectares in the 1996–2000 period to 37,763 hectares in the 2015–2021 period, while non-forested areas expanded from 44,004 hectares to 49,223 hectares during the same period. By 2021, forests constituted 42.4% of the study area, resulting in a loss of approximately 7397 hectares, which corresponds to 8.3% of the total area. Deforestation has primarily concentrated in the western part of the study area. The effects of deforestation are particularly evident near rural areas located far from the water reservoir. This indicates that there are actors and actions (especially related to land use) that influence the study area besides the hydropower reservoir. Consequently, the ten closest most affected rural areas in terms of forest loss area are Nain, Murmullo Alto, Maria de Jesus, Casajales, Kilometro 14, Zumbona, Chispas, La Osa, Alto Quimary, and Angostura (Figure 7). Evidence of forest recovery is observed in areas that are not associated with or adjacent to the intervention plots carried out by the company. This finding suggests the presence of ecological processes, e.g., natural succession, that are promoting restoration. It is important to note that, although the largest areas of forest recovery were detected in the year 2015, this does not necessarily imply that the recovery occurred specifically between 2010 and 2015. The visual inspection, which identified pastures in 1996, indicates that the recovery could have started before the previous period.

An accuracy assessment of the forest change map revealed variations in its performance across different time periods. The overall accuracy of the map consistently remained high for most of the periods, except in the 1996–2000 period, which had the lowest overall user's and producers' accuracies. This could be attributed to the Landsat 7 mission having a less frequent revisit rate compared to subsequent missions [5] and SLC-off malfunction [38,39]. As a result, it becomes challenging to produce cloud-free mosaics in tropical regions based on optical sensors, demonstrating the limitations of using optical sensors in tropical areas with high cloud cover [30] and the need to integrate active sensors for cloud-free EO data generation [5,10,14,15]. With the arrival of future missions, such as Landsat-8 and Landsat-9, the frequency of revisits increases, enhancing the probability of generating cloud-free mosaics. However, along with the information gaps caused by the SLC-off effect [38], these gaps in the data can be observed in mosaic generation with cloud and banding for the years 1996, 2000, 2005, and 2010; this can represent a limitation in the application of optic sensors to generate EO data for forest and deforestation monitoring in tropical and mountainous regions with a high frequency of clouds, especially during the rainy season. This was evident in the 1996 and 2000 mosaics, where certain areas lacked cloud-free pixels. Furthermore, since the first Landsat missions in 1972, several enhancements were made to improve the spatial, radiometric, and spectral resolutions [5]. These improvements can have varying effects on the final products, such as mosaics, which, in turn, can influence the accuracy assessment. The user's accuracy for the forest class also remained consistently high, ranging from 78% to 92%, indicating a high percentage of correctly classified forested pixels. The producer's accuracy for the forest class ranged from 96% to 100%, suggesting that the map accurately represented the distribution of forested

areas. Notably, the map showed a high level of effectiveness in detecting and representing deforestation events, with user's accuracies ranging from 90% to 99% and producer's accuracies ranging from 95% to 100% for the deforestation class. However, there were slight discrepancies in the representation of non-forested areas, with user's accuracies ranging from 97% to 100% and producer's accuracies ranging from 89% to 92%. These results demonstrate the overall high accuracy and reliability of the map in capturing land cover changes, particularly in detecting deforestation events. Nevertheless, there is room for improvement in accurately representing non-forested areas. Overall, the findings highlight the importance of regularly updating and refining classification methods to enhance the accuracy and precision of forest change maps.

The analysis of forested/non-forested dynamics and the time series analysis of the implementation plots revealed that three implementation plots reached a completed state, indicating successful forest restoration according to the provided definition. Furthermore, a small percentage (5.93%) of plots demonstrated an incipient restoration state, resembling grassland areas more than forests. Most evaluated plots (82.96%) were in an intermediate state, showing no significant differences compared to both grassland and forest reference data. Additionally, 10% of the plots displayed significant differences compared to grasslands but not forests, indicating an advanced state of reforestation.

4.2. Restoration Implementation Assessment Using Sentinel-1

When examining the implementation years, certain years showed a higher number of plots in the advanced state, such as 2018, 2016, 2013, and 2014. However, there was no statistically significant association between the restoration state and the implementation year, suggesting that the restoration status is not associated with the implementation year. The integration of additional variables associated with the type of implementations (active or passive) and species composition, among other factors, in conjunction with continuous vegetation structure time series provided by SAR data, could generate more insights for the evaluation of restoration process.

To effectively evaluate the success and impact of restoration strategies, it is crucial to combine on-the-ground data with remote sensing observations. Integrating these two sources of information allows for a comprehensive assessment of the restoration process, including the identification of factors that contribute to successful restoration and the identification of areas that may require further intervention. Implementing monitoring systems that integrate ground truth data and EO data enables a more robust and accurate evaluation of restoration efforts. By continuously assessing the progress and outcomes of restoration strategies, decision makers and stakeholders can make informed decisions regarding resource allocation, adaptive management, and the refinement of restoration approaches.

5. Conclusions

The proposed method for detecting and quantifying deforestation events using cloud-based and open-source science platforms proved to be effective in monitoring forest dynamics in the study area. The method allowed for the creation of composite images that facilitated the extraction of information-rich images, enabling the detection of spatially and quantitatively significant changes in forest coverage. The impacts of deforestation were particularly evident near rural areas, emphasizing the influence of actors and actions beyond the scope of the hydropower reservoir. However, this study also highlighted areas where forest recovery was observed, suggesting that the presence of ecological processes promote restoration.

The accuracy assessment of the forest change map demonstrated its high performance in detecting and representing deforestation events, with consistently high user's and producer's accuracies. While the accuracy for the forest class remained high, there were slight discrepancies in the representation of non-forested areas, indicating room for improvement. Regular updates and refinements to classification methods are crucial to enhance the accuracy and precision of forest change maps.

The analysis of implementation plots revealed that, currently, most of the implementation plots are in an intermediate state. Certain years showed a higher number of plots in an advanced state of reforestation, but no statistically significant association was found between the restoration state and the implementation year. The further integration of additional variables, such as the implementation type and species composition, along with continuous time series data from SAR, could provide deeper insights into the evaluation of the restoration process.

This research emphasizes that the application of these methods can be extended to tropical regions, and certain techniques can mitigate spatiotemporal gaps to produce annual mosaics. It is anticipated that integrating Landsat-7 may result in decreased accuracy due to its infrequent revisits and SLC-off malfunction. However, the reported lower accuracy estimates do not pose a significant issue when generating yearly mosaics inclusive of dry seasons. Yet, this limitation becomes pertinent when only imagery from the rainy season is integrated, necessitating the consideration of seasonality in future analyses.

To effectively evaluate the success and impact of restoration strategies, combining on-the-ground data with remote sensing observations is crucial. This integrated approach allows for a comprehensive assessment of the restoration process, aiding in the identification of factors contributing to successful restoration and areas requiring further intervention. By continuously monitoring and evaluating restoration efforts, decision makers and stakeholders can make informed decisions regarding resource allocation, adaptive management, and the refinement of restoration approaches.

Supplementary Materials: The following supporting information can be downloaded at: https://www.mdpi.com/article/10.3390/f15050754/s1, Figure S1: Number of restoration plots assessed grouped by implementation state and year of implementation; Table S1: Number of restoration plots assessed, grouped by implementation state and year if implementation.

References

1. Cabrera, E.; Vargas, D.M.; Galindo, G.; García, M.C.; Ordoñez, M.F. *Memoria Técnica de la Cuantificación de la Deforestación Histórica Nacional–Escalas Gruesa y Fina*; Instituto de Hidrología, Meteorología, y Estudios Ambientales-IDEAM: Bogotá, Colombia, 2011; p. 91.
2. Ustin, S.L.; Middleton, E.M. Current and Near-Term Advances in Earth Observation for Ecological Applications. *Ecol. Process.* **2021**, *10*, 1. [CrossRef] [PubMed]
3. Onoda, M.; Young, O.R. *Satellite Earth Observations and Their Impact on Society and Policy*; Springer: Singapore, 2017. [CrossRef]

4.   Hansen, M.C.; Stehman, S.V.; Potapov, P.V. Quantification of Global Gross Forest Cover Loss. *Proc. Natl. Acad. Sci. USA* **2010**, *107*, 8650–8655. [CrossRef] [PubMed]

5.   Reiche, J.; Lucas, R.; Mitchell, A.L.; Verbesselt, J.; Hoekman, D.H.; Haarpaintner, J.; Kellndorfer, J.M.; Rosenqvist, A.; Lehmann, E.A.; Woodcock, C.E.; et al. Combining Satellite Data for Better Tropical Forest Monitoring. *Nat. Clim. Chang.* **2016**, *6*, 120–122. [CrossRef]

6.   Mitchell, A.L.; Rosenqvist, A.; Mora, B. Current Remote Sensing Approaches to Monitoring Forest Degradation in Support of Countries Measurement, Reporting and Verification (MRV) Systems for REDD+. *Carbon Balance Manag.* **2017**, *12*, 9. [CrossRef] [PubMed]

7.   Lewis, S.L.; Edwards, D.P.; Galbraith, D. Increasing Human Dominance of Tropical Forests. *Science* **2015**, *349*, 827–832. [CrossRef]

8.   Murillo-Sandoval, P.J.; Kilbride, J.; Tellman, E.; Wrathall, D.; Van Den Hoek, J.; Kennedy, R.E. The Post-Conflict Expansion of Coca Farming and Illicit Cattle Ranching in Colombia. *Sci. Rep.* **2023**, *13*, 1965. [CrossRef]

9.   Joshi, N.; Mitchard, E.T.A.; Woo, N.; Torres, J.; Moll-Rocek, J.; Ehammer, A.; Collins, M.; Jepsen, M.R.; Fensholt, R. Mapping Dynamics of Deforestation and Forest Degradation in Tropical Forests Using Radar Satellite Data. *Environ. Res. Lett.* **2015**, *10*, 34014. [CrossRef]

10.   Joshi, N.; Baumann, M.; Ehammer, A.; Fensholt, R.; Grogan, K.; Hostert, P.; Jepsen, M.R.; Kuemmerle, T.; Meyfroidt, P.; Mitchard, E.T.A.; et al. A Review of the Application of Optical and Radar Remote Sensing Data Fusion to Land Use Mapping and Monitoring. *Remote Sens.* **2016**, *8*, 70. [CrossRef]

11.   van Oostende, M.; Hieronymi, M.; Krasemann, H.; Baschek, B.; Röttgers, R. Correction of Inter-Mission Inconsistencies in Merged Ocean Colour Satellite Data. *Front. Remote Sens.* **2022**, *3*, 882418. [CrossRef]

12.   Shimada, M.; Itoh, T.; Motooka, T.; Watanabe, M.; Shiraishi, T.; Thapa, R.; Lucas, R. New Global Forest/Non-Forest Maps from ALOS PALSAR Data (2007–2010). *Remote Sens. Environ.* **2014**, *155*, 13–31. [CrossRef]

13.   Lucas, R.; Rebelo, L.M.; Fatoyinbo, L.; Rosenqvist, A.; Itoh, T.; Shimada, M.; Simard, M.; Souza-Filho, P.W.; Thomas, N.; Trettin, C.; et al. Contribution of L-Band SAR to Systematic Global Mangrove Monitoring. *Mar. Freshw. Res.* **2014**, *65*, 589–603. [CrossRef]

14.   Persaud, H.; Cabrera, I. Eficiencia de Las Imágenes de Radar Para El Monitoreo a Tiempo Casi Real de Bosques Tropicales En Guyana. *Arnaldoa* **2021**, *28*, 577–592. Available online: http://www.scielo.org.pe/scielo.php?pid=S2413-32992021000300577&script=sci_arttext (accessed on 11 December 2023).

15.   Palomino-Ángel, S.; Anaya-Acevedo, J.A.; Simard, M.; Liao, T.-H.; Jaramillo, F. Analysis of Floodplain Dynamics in the Atrato River Colombia Using SAR Interferometry. *Water* **2019**, *11*, 875. [CrossRef]

16.   Estupinan-Suarez, L.M.; Florez-Ayala, C.; Quinones, M.J.; Pacheco, A.M.; Santos, A.C. Detection and Characterizacion of Colombian Wetlands Using Alos Palsar and MODIS Imagery. *Int. Arch. Photogramm. Remote Sens. Spatial Inf. Sci.* **2015**, *XL-7/W3*, 375–382. [CrossRef]

17.   Ayala, C.F.; Suárez, L.M.E.; Rojas, S.; Aponte, C. Identification and Mapping of Colombian Inland Wetlands. *Biota Colomb.* **2016**, *17*, 1–22. Available online: http://repository.humboldt.org.co/handle/20.500.11761/9352 (accessed on 9 September 2023).

18.   Hoekman, D.H.; Quinones, M.J. Land Cover Type and Forest Biomass Assessment in the Colombian Amazon. In Proceedings of the IGARSS'97, 1997 IEEE International Geoscience and Remote Sensing Symposium Proceedings. Remote Sensing-A Scientific Vision for Sustainable Development, Singapore, 3–8 August 1997.

19.   Hoekman, D.H.; Quinones, M.J. Land Cover Type and Biomass Classification Using AirSAR Data for Evaluation of Monitoring Scenarios in the Colombian Amazon. *IEEE Trans. Geosci. Remote Sens.* **2000**, *38*, 685–696. [CrossRef]

20.   Anaya, J.A.; Rodríguez-Buriticá, S.; Londoño, M.C. Clasificación de cobertura vegetal con resolución espacial de 10 metros en bosques del Caribe colombiano basado en misiones Sentinel 1 y 2. *Rev. Teledetec.* **2023**, 29–41. [CrossRef]

21.   Hoekman, D.; Quiñones, M.J. Biophysical Forest Type Characterization in the Colombian Amazon by Airborne Polarimetric SAR. *IEEE Trans. Geosci. Remote Sens.* **2002**, *40*, 1288–1300. [CrossRef]

22.   Quiñones, M.J.; Vissers, M.; Pacheco-Pascaza, A.M.; Flórez, C.; Estupiñán-Suárez, L.M.; César, A.; Úrsula, J.; Claudia, H.; Dirk, H. Un enfoque ecosistémico para el análisis de una serie densa de tiempo de imágenes de radar Alos PALSAR, para el mapeo de zonas inundadas en el territorio continental colombiano. *Biota Colomb.* **2016**, *16*, 63–84. [CrossRef]

23.   Pedraza, C.; Clerici, N.; Forero, C.F.; Melo, A.; Navarrete, D.; Lizcano, D.; Zuluaga, A.F.; Delgado, J.; Galindo, G. Zero Deforestation Agreement Assessment at Farm Level in Colombia Using ALOS PALSAR. *Remote Sens.* **2018**, *10*, 1464. [CrossRef]

24.   Anaya, J.A.; Gutiérrez-Vélez, V.H.; Pacheco-Pascagaza, A.M.; Palomino-Ángel, S.; Han, N.; Balzter, H. Drivers of Forest Loss in a Megadiverse Hotspot on the Pacific Coast of Colombia. *Remote Sens.* **2020**, *12*, 1235. [CrossRef]

25.   Klemas, V. Using Remote Sensing to Select and Monitor Wetland Restoration Sites: An Overview. *J. Coast. Res.* **2013**, *289*, 958–970. [CrossRef]

26.   Reif, M.K.; Theel, H.J. Remote Sensing for Restoration Ecology: Application for Restoring Degraded, Damaged, Transformed, or Destroyed Ecosystems. *Integr. Environ. Assess. Manag.* **2017**, *13*, 614–630. [CrossRef] [PubMed]

27.   Camarretta, N.; Harrison, P.A.; Bailey, T.; Potts, B.; Lucieer, A.; Davidson, N.; Hunt, M. Monitoring Forest Structure to Guide Adaptive Management of Forest Restoration: A Review of Remote Sensing Approaches. *New For.* **2020**, *51*, 573–596. [CrossRef]

28.   Xie, L.; Wu, W.; Huang, X.; Ou, P.; Lin, Z.; Zhiling, W.; Song, Y.; Lang, T.; Huangfu, W.; Zhang, Y.; et al. Mining and Restoration Monitoring of Rare Earth Element (REE) Exploitation by New Remote Sensing Indicators in Southern Jiangxi, China. *Remote Sens.* **2020**, *12*, 3558. [CrossRef]

29.   Koch, A.; Kaplan, J.O. Tropical Forest Restoration under Future Climate Change. *Nat. Clim. Chang.* **2022**, *12*, 279–283. [CrossRef]

30. Rodriguez, N.; Armenteras, D.; Morales, M.; Romero, M. *Ecosistemas de Los Andes Colombianos*; Instituto de Investigación de Recursos Biológicos Alexander von Humboldt: Bogotá, Colombia, 2006.

31. Masek, J.G.; Wulder, M.A.; Markham, B.; McCorkel, J.; Crawford, C.J.; Storey, J.; Jenstrom, D.T. Landsat 9: Empowering Open Science and Applications through Continuity. *Remote Sens. Environ.* **2020**, *248*, 111968. [CrossRef]

32. Helder, D.L.; Karki, S.; Bhatt, R.; Micijevic, E.; Aaron, D.; Jasinski, B. Radiometric Calibration of the Jandsat MSS Sensor Series. *IEEE Trans. Geosci. Remote Sens.* **2012**, *50*, 2380–2399. [CrossRef]

33. Li, J.; Roy, D.P. A Global Analysis of Sentinel-2a, Sentinel-2b and Landsat-8 Data Revisit Intervals and Implications for Terrestrial Monitoring. *Remote Sens.* **2017**, *9*, 902. [CrossRef]

34. Prudente, V.H.R.; Martins, V.S.; Vieira, D.C.; Silva, N.R.d.F.e.; Adami, M.; Sanches, I.D.A. Limitations of Cloud Cover for Optical Remote Sensing of Agricultural Areas across South America. *Remote Sens. Appl. Soc. Environ.* **2020**, *20*, 100414. [CrossRef]

35. Jafarbiglu, H.; Pourreza, A. Impact of Sun-View Geometry on Canopy Spectral Reflectance Variability. *ISPRS J. Photogramm. Remote Sens.* **2023**, *196*, 270–286. [CrossRef]

36. Asner, G.P. Automated Mapping of Tropical Deforestation and Forest Degradation: CLASlite. *J. Appl. Remote Sens.* **2009**, *3*, 033543. [CrossRef]

37. Nielsen, A.; Conradsen, K.; Simpson, J.J. Multivariate Alteration Detection (MAD) in Multispectral, Bi-Temporal Image Data: A New Approach to Change Detection Studies. *Remote Sens. Environ.* **1998**, *1*, 1–28. [CrossRef]

38. Rahaman, K.; Hassan, Q.; Ahmed, M. Pan-Sharpening of Landsat-8 Images and Its Application in Calculating Vegetation Greenness and Canopy Water Contents. *ISPRS Int. J. Geo-Inf.* **2017**, *6*, 168. [CrossRef]

39. Storey, J.; Scaramuzza, P.; Schmidt, G.; Barsi, J. Landsat 7 scan line corrector-off gap-filled product development. *Proceeding Pecora* **2005**, *16*, 23–27.

40. Werner, C.; Wegmüller, U.; Strozzi, T.; Wiesmann, A. *GAMMA SAR and Interferometric Processing Software*; European Space Agency (Special Publication) ESA SP.: São Paulo, Brazil, 2000; No. 461; pp. 211–219.

41. Lopes, A.; Touzi, R.; Nezry, E. Adaptive Speckle Filters and Scene Heterogeneity. *IEEE Trans. Geosci. Remote Sens.* **1990**, *28*, 992–1000. [CrossRef]

42. Galindo, G.; Espejo, O.J.; Rubiano, J.C.; Vergara, L.K.; Cabrera, E. *Protocolo de Procesamiento Digital de Imágenes Para La Cuantificación de La Deforestacion En Colombia V.2*; IDEAM, Instituto de Hidrología, Metereología y Estudios Ambientales: Bogotá, Colombia, 2014; pp. 1–225. [CrossRef]

43. Baranwal, A.; Bagwe, B.R.; Vanitha, M. Machine Learning in Python. *J. Mach. Learn. Res.* **2019**, *12*, 128–154. [CrossRef]

44. Tatsumi, K.; Yamashiki, Y.; Canales Torres, M.A.; Taipe, C.L.R. Crop Classification of Upland Fields Using Random Forest of Time-Series Landsat 7 ETM+ Data. *Comput. Electron. Agric.* **2015**, *115*, 171–179. [CrossRef]

45. Wang, J.; Zhao, Y.; Li, C.; Yu, L.; Liu, D.; Gong, P. Mapping Global Land Cover in 2001 and 2010 with Spatial-Temporal Consistency at 250m Resolution. *ISPRS J. Photogramm. Remote Sens.* **2015**, *103*, 38–47. [CrossRef]

46. Pal, M. Random forests for land cover classification. Mahesh Pal Department of civil engineering National Institute of technology, Kurukshetra. *Symp. A Q. J. Mod. Foreign Lit.* **1996**, *26*, 3510–3512. [CrossRef]

47. Teluguntla, P.; Thenkabail, P.S.; Oliphant, A.; Xiong, J.; Gumma, M.K.; Congalton, R.G.; Yadav, K.; Huete, A. A 30-m Landsat-Derived Cropland Extent Product of Australia and China Using Random Forest Machine Learning Algorithm on Google Earth Engine Cloud Computing Platform. *ISPRS J. Photogramm. Remote Sens.* **2018**, *144*, 325–340. [CrossRef]

48. Deng, J.S.; Wang, K.; Deng, Y.H.; Qi, G.J. PCA-based Land-use Change Detection and Analysis Using Multitemporal and Multisensor Satellite Data. *Int. J. Remote Sens.* **2008**, *29*, 4823–4838. [CrossRef]

49. DeFries, R.; Achard, F.; Brown, S.; Herold, M.; Murdiyarso, D.; Schlamadinger, B.; De Souza, C. Earth Observations for Estimating Greenhouse Gas Emissions from Deforestation in Developing Countries. *Environ. Sci. Policy* **2007**, *10*, 385–394. [CrossRef]

50. Olofsson, P.; Foody, G.M.; Stehman, S.V.; Woodcock, C.E. Making Better Use of Accuracy Data in Land Change Studies: Estimating Accuracy and Area and Quantifying Uncertainty Using Stratified Estimation. *Remote Sens. Environ.* **2013**, *129*, 122–131. [CrossRef]

51. Ruiz-Ramos, J.; Marino, A.; Boardman, C.; Suarez, J. Continuous Forest Monitoring Using Cumulative Sums of Sentinel-1 Timeseries. *Remote Sens.* **2020**, *12*, 3061. [CrossRef]

52. Urrea, V.; Ochoa, A.; Mesa, O. Seasonality of Rainfall in Colombia. *Water Resour. Res.* **2019**, *55*, 4149–4162. [CrossRef]

53. Susan Moran, M. Principles and Applications of Imaging Radar, Manual of Remote Sensing, 3rd Edition, Volume 2. *Eos Trans. Am. Geophys. Union* **1999**, *80*, 67.

54. Rüetschi, M.; Small, D.; Waser, L. Rapid Detection of Windthrows Using Sentinel-1 C-Band SAR Data. *Remote Sens.* **2019**, *11*, 115. [CrossRef]

55. Eriksson, L.E.B.; Fransson, J.E.S.; Soja, M.J.; Santoro, M. Backscatter Signatures of Wind-Thrown Forest in Satellite SAR Images. In Proceedings of the 2012 IEEE International Geoscience and Remote Sensing Symposium, Munich, Germany, 22–27 July 2012; IEEE: Munich, Germany, 2012; pp. 6435–6438. [CrossRef]

56. Kasischke, E.S.; Melack, J.M.; Dobson, M.C. The Use of Imaging Radars for Ecological Applications—A Review. *Remote Sens. Environ.* **1997**, *59*, 141–156. [CrossRef]
57. Flores, A.; Herndon, K.; Thapa, R.; Cherrington, E. *Synthetic Aperture Radar (SAR) Handbook: Comprehensive Methodologies for Forest Monitoring and Biomass Estimation*; Alabama University Huntsville: Huntsville, AL, USA, 2019. [CrossRef]